Aeronautical Research Institute, University of Tokyo
Report No. 341, March 1959

Experimental Study on the Supersonic Flow Around Blunt-Nosed Bodies of Revolution

By

Hakuro OGUCHI

Summary. The flows around several blunt-nosed bodies of revolution were experimentally investigated over the Mach number range from 3.76 to 4.78 at the intermittent blow-down type supersonic wind tunnel of Aeronautical Research Institute, University of Tokyo. In the present experiment we are concerned with the flow behavior ahead of the bodies so that the interferometric study was primarily made.

The main results are summarized as follows:

(1) The surface pressure referred to the stagnation pressure, shock-wave pattern, sonic-line pattern and flow directions were found to be closely correlated to those found both experimentally and theoretically for the case of the flow with the much higher Mach number than in the present test.

(2) The region with the local Mach number lower than 0.5 was confirmed to spread extensively ahead of the nose.

(3) The shock-wave detachment distance was found to be nearly independent of the nose shape, when referred to the radius of curvature of the shock wave.

(4) For the bodies with the same nose radius, the shock-wave detachment distances were found to be nearly independent of the position of the body shoulders.

1. INTRODUCTION

For a hypersonic flight a blunt-nosed body is of more practical interest than a sharp-nosed body, because the heat transfer at the nose, being greater than anywhere on the surface, can be appreciably reduced by its use. For that reason, the flow over a blunt-nosed body has received a considerable amount of attention by many authors.

In the recent paper [*1*], we put forward an analytical method for the problem when a spherical body is placed in a hypersonic flow. This method makes it possible to treat the problem when the viscous layer is so thick that the disturbed flow field can be no longer divided distinctly into the inviscid and viscous regions. In the course of the analysis, however, several simplifying assumptions were made in order to avoid anomalous difficulties to be met in the full treatment of the problem. Most important one of these assumptions is that the flow is incompressible behind the shock wave. This simplification which makes the analysis easy was already applied by Li and Geiger [*2*], by Lighthill [*3*] and by Hida [*4*] in their inviscid flow analyses of the same problem. In the present experi-

mental study we are concerned partly with the examination of the above-mentioned simplification.

The experiment was done at the intermittent blow-down type 5×10 cm supersonic wind tunnel of Aeronautical Research Institute, University of Tokyo. The tunnel was equipped with the variable nozzle and diffuser in such a way that the test Mach number covers continuously the range from 3.76 to 4.78. The flows over several blunt bodies of revolution were investigated (Fig. 1 and Plate 1).

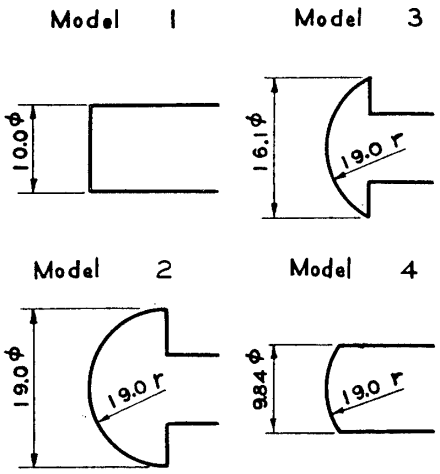

(The measurements are in mm)

FIGURE 1.

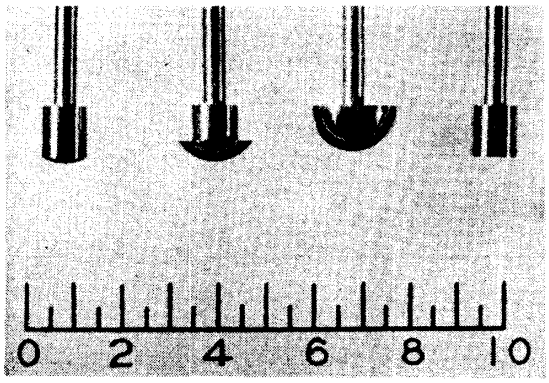

PLATE 1.

The experimental studies on the flow over a blunt-nosed body of revolution at hypersonic flight speeds were worked out by Oliver [5] and by Erassa and Wisenbaker* at GALCIT hypersonic wind tunnel, by Vas, Bogdonoff and Hammitt [7] at Princeton helium tunnel and by others (for example, see the works cited in References [6] and [8]).

The ratios of the surface pressure to the stagnation one, measured for the flat-nosed cylinder and hemisphere at the free-stream Mach number 4.3, have been found in an excellent agreement with those measured in GALCIT hypersonic tunnel at the free-stream Mach number 5.8 [5] [6]. Moreover, from the detail survey by means of the Mach-Zehender interferometer, the flow directions and sonic line location in the flow over a sphere have been found to be closely correlated to those obtained numerically in Reference [10] for a nearly spherical body placed at the free-stream Mach number 5.8. From these results, we may say that the Mach numbers in the present experiment are not so low to investigate some of the characteristic features pertinent to a hypersonic flow around the blunt-nosed body of revolution. Previously Oswatitsch [9] suggested on the basis of the drag data of the sphere the occurrence of characteristic features pertinent to hypersonic flow at lower Mach number than anticipated usually. For this reason we are concerned primarily with characteristic features of the flow pat-

* Their work was introduced by Lees in his paper [6].

tern over the blunt-nosed body of revolution when placed in high supersonic flows.

2. Wind Tunnel and Facilities for Variable Test Mach Number

The supersonic flow was established at the test section by discharging the atmospheric air compressed in the reservoir at the pressure up to 200 atms., into the atmosphere through the settling chamber by regulating the valve manually.

The variable-geometry nozzle and diffuser were designed in such a way that the test Mach number can be changed during the tunnel run (Plate 2). The nozzle has a Foelsch's contour computed for the Mach number 5.0 and for the test section with the sectional area 5×10 cm^2. In the determination of the present nozzle contour, the effect of the boundary-layer displacement was not all taken into account.

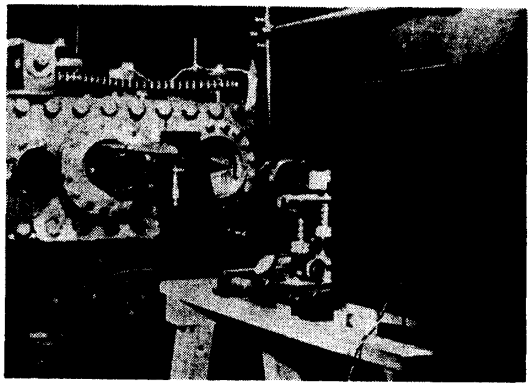

Plate 2.

The upper-side nozzle block was mounted on the tunnel wall in such a way as to move from the throat opening 11.22 mm to fully closing in the direction perpendicular to the tunnel axis. As shown in Plate 2, its motion is produced by a 1/2 HP motor that is connected with the nozzle through the wheel, chain and three jacks. The upper-side diffuser plate after the movable nozzle block was deformable by the manual operation of three jacks over the diffuser-throat opening range from 76.3 to 37.8 mm. The lower sides of both nozzle and diffuser have fixed geometries, that is, the former has, as mentioned before, the Foelsch's contour for Mach number 5.0 and the latter a nearly circular arc. The flexible diffuser part could be adjusted so as to hold always its contour nearly in circular arc.

In the present test the supply pressure was restricted up to 18 kg/cm^{2}g from the structural reason of the flexible part of diffuser. As is well known, the pressure ratio p_0/p_e (p_0; supply pressure, p_e; exit pressure) needed for the tunnel start is independent of the diffuser so far as the viscosity effect may be neglected. After the flow has been established, however, it can be maintained at lower pressure ratio than that needed for the start. In general there exists a minimum pressure ratio $(p_0/p_e)_{\text{mini.}}$ for the maintenance of the tunnel run, its value being

dependent primarily upon the diffuser. According to the one dimensional consideration, this minimum pressure ratio $(p_0/p_e)_{\text{mini.}}$ may be determined only from the ratio, Ψ, of the test-section area to the diffuser throat area. Since, in fact, the phenomenon becomes more complicated due to the viscosity effect of the fluid together with two-dimensional effect, the ratio $(p_0/p_e)_{\text{mini.}}$ depends not only on the value of Ψ but also on the overall geometry of the diffuser. For the nozzle-diffuser combination used for the present test, the values of $(p_0/p_e)_{\text{mini.}}$ are plotted in Fig. 2 against the values of Ψ. These results were obtained for the case where any model is not set at the test section. For the case where the model is set,

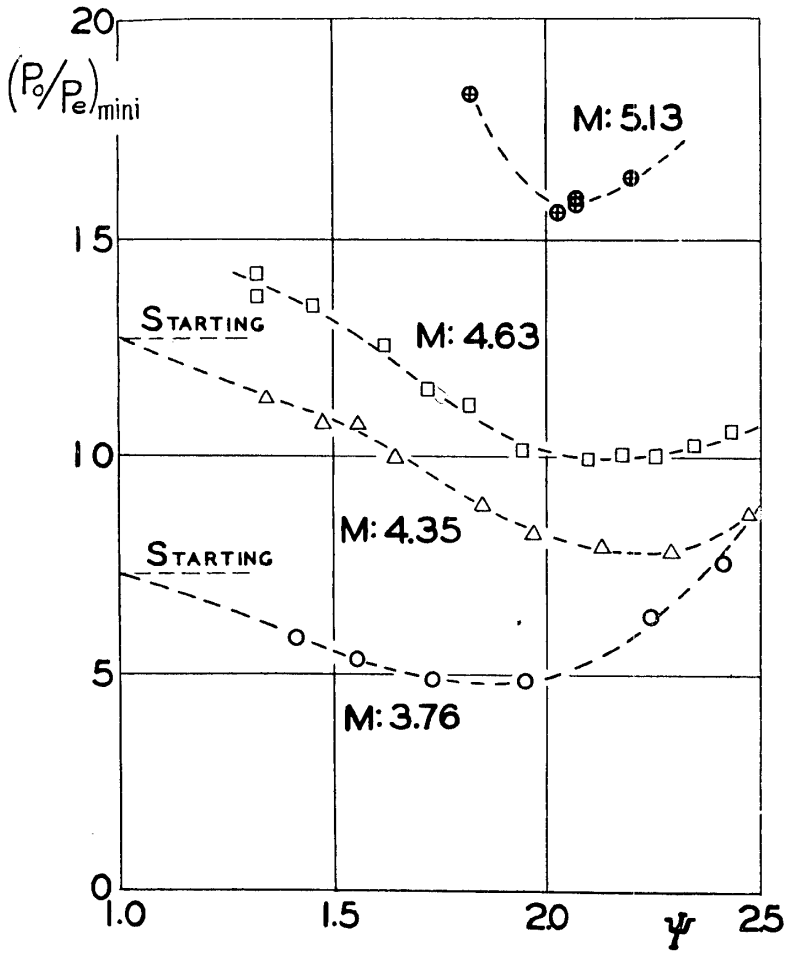

FIGURE 2. Minimum running pressure ratio versus diffuser contraction ration Ψ.

the diffuser performance may be different from that for no-model case, but may be considered to behave in a similar manner.

Consider, now, that the supply pressure ratio p_0/p_e is initially given. Then, as seen from the diffuser performance presented in Fig. 2, there may exist a test Mach number, in which the initially given pressure ratio is just a minimum one. This Mach number is the maximum one to be achieved for the given pressure ratio. In the present test the flow with the test Mach number 3.76 was obtained in the fully opening of the nozzle throat and then the pressure 6.5 kg/cm^{2}g was

initially needed for the tunnel start. Therefore, when a certain supply pressure above 6.5 kg/cm^{2}g is initially given, we can attain to an optimum Mach number, in which the supply pressure ratio may be identified with the minimum one, by simultaneous adjustment of nozzle and diffuser. Indeed, the flows with the test Mach number up to 4.78 were achieved for the supply pressure up to 18 kg/cm^{2}g. The further detail of such an operation was already provided by the present author in Reference [*11*].

3. Flow Measurements by Optical Methods

As is well known, the Mach-Zehender interferometer is the most suitable instrument to the quantitative investigation of the flow. The theory of the Mach-Zehender interferometer has been given by various authors (see, for example, [*12*] [*13*]). As shown in Plate 2, the interferometer used rests on the angle iron and the four plates are equipped with this angle iron in such a way that a plane involving their centers is vertical to the tunnel axis which is horizontal. The overall arrangement of the Mach-Zehender interferometer is sketched in Fig. 3. The light emitted from the mercury lamp was made monochromatic with a colour filter V-GIA that intercepts all lines except a green line 5641 Å. The light from the light source is converted into a parallel beam by a lense L_2 and then split into two mutually perpendicular beams by the half-reflecting plate S_1. One beam

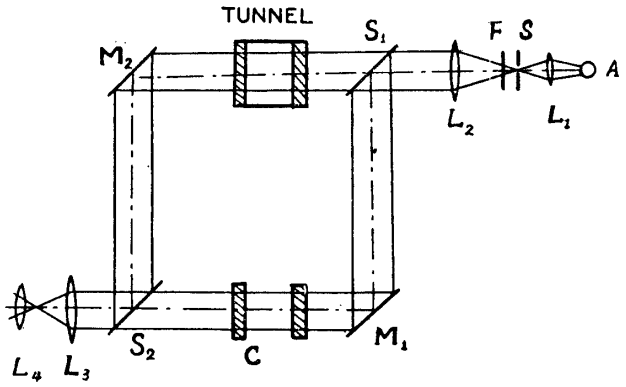

FIGURE 3. Schematic diagram of M–Z interferometer.

passes through the wind tunnel and then is reflected by the mirror M_2. Another beam is reflected by the mirror M_1 and then passes through the compensating chamber which is used to produce equal optical paths in glass. The two beams are reunited at the half-reflecting plate S_2. If there is an appropriate difference between the optical paths through S_1, M_2 and S_2 and through S_1, M_1 and S_2, then the interference fringes will be produced in any plane. The test plane and the interference fringes there are focused on the photographic plate by two lenses L_3 and L_4 so that the interferogram may be taken for analysis. In practice, this can be done by suitable adjustments of the half-reflecting plates and mirrors, which can be rotated by screws around any axis and moved in the direction perpendicular to the surfaces, respectively.

The refractive index, n, of the gas is related to the density of the gas by the equation suggested by Gladstone and Dale as follows:

$$\frac{n-1}{\rho}=K,$$

where K is a constant for the gas used. Since the velocity, c, of light is

$$c=\frac{1}{n}c^*,$$

where c^* is the velocity in *vaccuo*, it depends only upon the density of the medium. Therefore the change in density of the flow in test plane results in the optical path difference between the two paths, that is, S_1–M_2–S_2 and S_1–M_1–S_2, and thus the interferometric fringe shifts occur. Therefore, the interferometric fringe shifts are immediately related to the change in density at the test plane. The evaluation of the density from the interferogram will be mentioned later, and in this section we does not proceed into further detail of the theory of the interferometer. Here the dimensions of the main parts used are summarized as follows:

the lense L_2; focal distance 18 cm,
the lense L_3; focal distance 60 cm,
the plates; diameter 120 mm and thickness 20 mm.

The schlieren observation can be made by intercepting the light passing through M_1 and, furthermore, by setting a slit at the focus of the lense L_3. The schlieren method, which depends upon the gradient of the refractive index and thus upon that of the density, is suitable to the qualitative study of the flow pattern. In the present experiment the shock-wave patterns were observed by both interferometer and schlieren method.

4. Characteristics of the Wind Tunnel

The Mach numbers of the test flow were determined from both of the pitot pressure and the density obtained by the interferometer. The pitot pressures p_0' were measured by reading the indications of the mercury manometer led to the pitot tube whose outer and inner diameters are 2 mm and 1.4 mm, respectively. The stagnation pressures, p_0, of the test flows were measured with the Bourdon gauge attached to the settling chamber. Then the Mach numbers were evaluated by using the relation as follows:

$$\frac{p_0'}{p_0}=\left[\frac{(\gamma+1)M^2}{2}\right]^{\frac{\gamma}{\gamma-1}}\left[\frac{\gamma+1}{2\gamma M^2(\gamma-1)}\right]^{\frac{1}{\gamma-1}},$$

where γ is the ratio of the specific heats of gas (see, for example, [*14*]).

As shown before, the density, ρ, of the gas is related to the refractive index n by the equation suggested by Gladstone and Dale. Consider, now, that the wind tunnel is filled up with the surrounding atmosphere, and the interference fringes there are visible on the photographic plate. Then, if the flow is established in

the tunnel, the fringe shift will be produced.

For the two-dimensional flow phenomena, the density may be assumed constant along the light path in the tunnel so that the flow density can easily be evaluated from the fringe shift in the following way. Let δ be the ratio of the fringe shift to the fringe interval (it being usually termed simply the fringe shift), λ the wave length of the light used and L the wind-tunnel width, then

$$\delta\lambda=(n-n_a)L=KL(\rho-\rho_a),$$

where the subscript a represents the quantities at the surrounding atmosphere in reference. That is, the density ρ is given by

$$\rho-\rho_a=\lambda\delta/KL. \qquad (1)$$

To obtain the fringe shift, a particular fringe must be identified. This is, however, considerably difficult for the interferogram produced by a monochromatic light from the mercury lamp with constant intensity. For this case the use of white light is profitable to make the discrimination of each fringe feasible, because it gives few fringes sufficiently to identify the zero-order fringe. Since the zero-order fringe appears at the center of interference, we can distinctly identify the zero-order fringes in the pictures taken for monochromatic light as

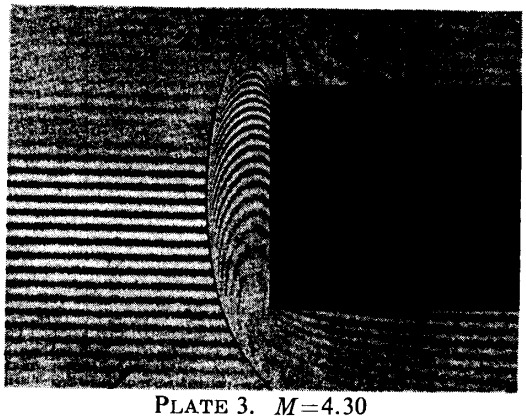

PLATE 3. $M=4.30$

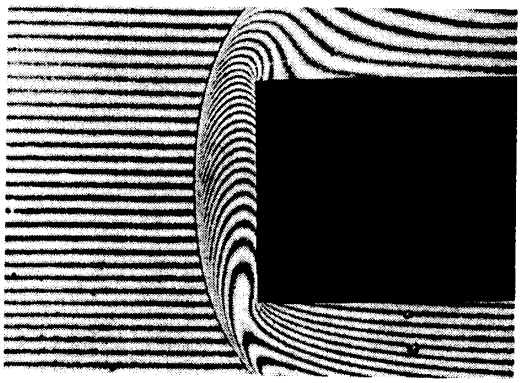

PLATE 4. $M=4.30$

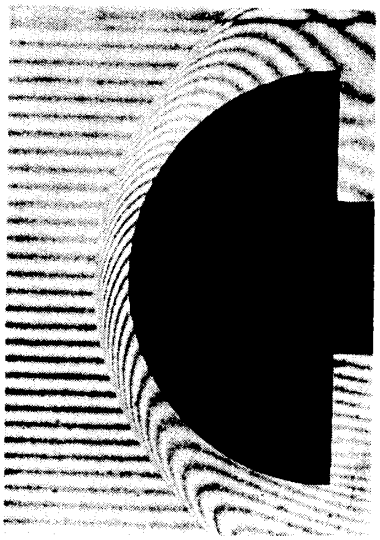

PLATE 5. $M=4.30$

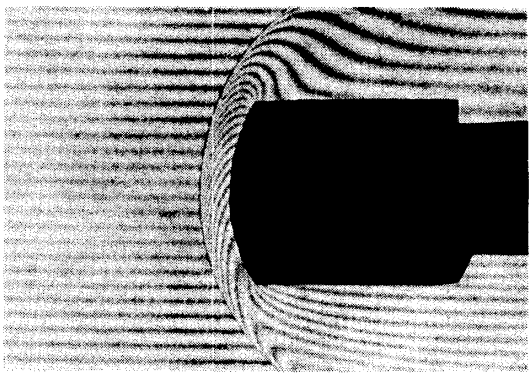

PLATE 6. $M=4.30$

compared with the corresponding pictures taken for white light source (see, for example, Plates 3 and 4). Therefore, we can number the fringes and evaluate the fringe shifts at the field under investigation. The use of white light source is also convenient for the investigation of the flow field with such a discontinuity as a shock wave.

Since the undisturbed flow may be considered two dimensional, the density there is easily evaluated from Eq. (1) in the above-mentioned way. Then the test Mach number can be determined by use of the relation as follows:

$$\frac{\rho}{\rho_0}=\left(1+\frac{\gamma-1}{2}M^2\right)^{-\frac{\gamma}{\gamma-1}},$$

where ρ_0 is the density at the stagnation condition.

The free-stream Mach numbers determined from either the pitot pressure or the density are plotted in Fig. 4 against the nozzle-throat height in mm. Here the nozzle-throat height was measured within the accuracy of 0.04 mm by recording, with the counter, rotations of the wheel mounted on the movable nozzle block. The free stream may be considered sufficiently uniform over the visible range on the photographic plate, because only slight distortion of the fringes was found there (see, for example, Plates 4–6).

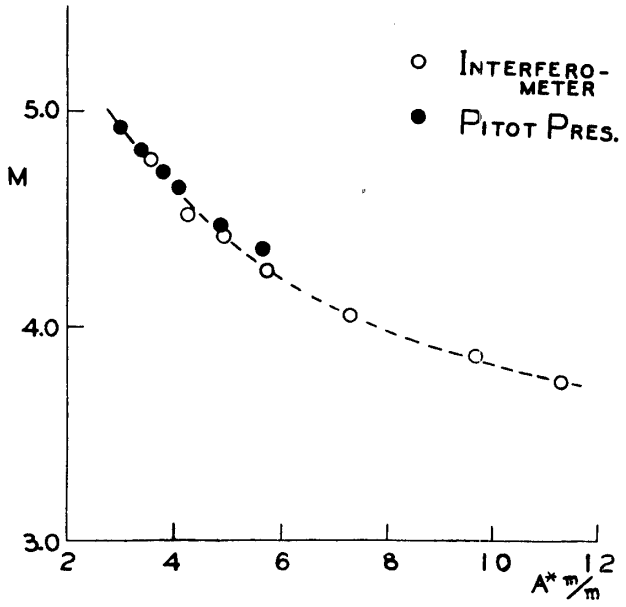

FIGURE 4. Test-section Mach number M versus throat height A^*.

Any equipment was not especially set up to dry the atmospheric air, but the greater part of humidity in air was removed at the oil-water separator before going into the storage. Indeed, the humidity measured at the settling chamber was within the range of dew point from -33 to -43°C.

Since the air in the settling chamber is nearly at rest, the condition at the settling chamber may be assumed as the stagnation condition of the test flow. Thus

the stagnation temperature was known by measuring the temperature at the settling chamber by means of the Cu-Co thermojunction.

According to the Sutherland's formula, the viscosity coefficient can be expressed in the form

$$\mu=\text{const.}\times T^{1.5}/(T+C),$$

where the temperature T is in Kelvin, and C is a constant and 114°K for the air.

The free-stream Reynolds number based on a given length l is

$$R_e=\frac{U\rho l}{\mu},$$

where U is the free-stream velocity. Let the quantities at the stagnation condition be identified by subscript 0. Then (see, for example, [*13*]).

$$R_e=\frac{a_0 l\rho_0[T_0/\{1+\frac{1}{2}(\gamma-1)M^2\}C]}{\mu_0[1+\frac{1}{2}(\gamma-1)M^2]^{(3-\gamma)/(\gamma-1)}(T_0+C)},$$

where a_0 is the sound speed at the stagnation. In the present test the measured stagnation temperatures were found within the range from -8 to 10°C and the Reynolds number per cm was within the range from 6×10^5 to 8×10^5.

5. Evaluation of the Density from the Interferograms for the Case When the Flow is Axially Symmetric

In the present test all of the models were set with no angle of attack to the free-stream direction. The models used are of axially symmetric form and thus so are the flow fields. The following four sorts of models were selected for the test; (1) a flat-nosed cylinder with the diameter 10 mm (Model 1), (2) a hemisphere with a radius of 19mm (Model 2) and (3) two hemispheres with same radius as Model 2, cut off in such a way that the diameters of the maximum cross section are 16.1 mm and 9.84 mm, respectively, these being designated as Models 3 and 4 (Fig. 1).

In the present test the shock waves always occur ahead of the body and the disturbed region is confined within the range between the shock wave and the body. For such an axially symmetric phenomena, the density changes along the optical path in the disturbed region so that the evaluation of the density from interferogram becomes very troublesome as compared with that for the two-dimensional case.

Let us now investigate, for the case of the axially symmetric flow, how to evaluate the density from the interferogram. A certain cross section vertical to the body axis is shown in Fig. 5. In this plane let the Cartesian coordinates (X, Y) be chosen in such a way that X direction is parallel to the light path and Y direction normal to it, r be radial distance from the axis and $r=R$ represent the shock-wave location. Since, as mentioned before, the density of the undisturbed flow ahead of the shock wave is easily obtained, it may now be chosen as a re-

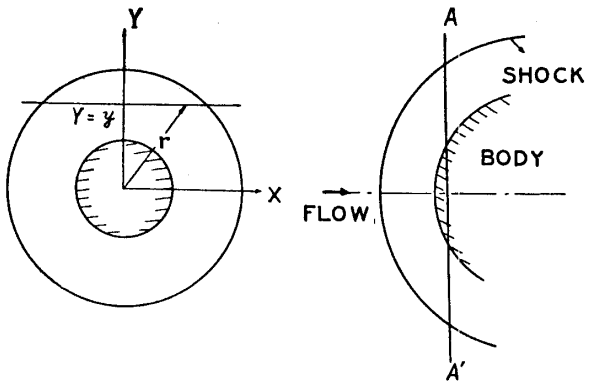

FIGUER 5.

ference density. Then the shift, δ^*, of the disturbed flow fringe referred to the free-stream fringe is given by [*15*]

$$\delta^*\lambda=2\int_y^R [n(r)-n_1]\frac{rdr}{(r^2-y^2)^{1/2}}$$
$$=2\int_y^R \nu(r)\frac{rdr}{(r^2-y^2)^{1/2}},$$

where the subscript 1 represents the quantity at the reference field or undisturbed flow field, and with the abbreviation

$$\nu=n-n_1.$$

It is now convenient to introduce the following variables suggested by J. von Neumann [*15*],

$$v=r^2, \qquad u=y^2.$$

Then the above integral equation is reduced to the Abel's equation i.e.,

$$\lambda\delta^*(u)=\int_u^{R^2}\frac{\nu(v)}{(v-u)^{1/2}}dv. \tag{2}$$

The solution ν of this integral equation is easily obtained in the following way. Let us introduce the variables x, ξ by the transformation

$$R^2-v=x, \qquad R^2-u=\xi, \tag{3}$$

then Eq. (2) becomes

$$\lambda\Delta(\xi)=\int_0^{\xi}\frac{\mu(x)}{(\xi-x)^{1/2}}dx, \tag{4}$$

where the functions Δ and μ are defined by

$$\left.\begin{aligned}\Delta(\xi)&=\delta^*(R^2-\xi),\\ \mu(x)&=\nu(R^2-x).\end{aligned}\right\} \tag{5}$$

It is well known from the the theory of integral equation that, when the unknown function f is related to the known function u as follows:

$$f(x)=\int_0^x\frac{u(\xi)}{(x-\xi)^{\alpha}}d\xi, \qquad 0<\alpha<1, \tag{6}$$

it is given by

$$u(z)=\frac{\sin\pi\alpha}{\pi}\frac{d}{dz}\int_0^z\frac{f(x)}{(z-x)^{1-\alpha}}dx$$

or

$$u(z)=\frac{\sin\pi\alpha}{\pi}\int_0^z\frac{f'(\xi)}{(z-\xi)^{1-\alpha}}d\xi\,, \tag{7}$$

where the prime denotes the differentiation with respect to the argument. Applying the above theorem to Eq. (4), we obtain

$$\mu(x)=\frac{\lambda}{\pi}\int_0^x\frac{\Delta'(\xi)}{(x-\xi)^{1/2}}d\xi\,.$$

From the definition (5) of the functions Δ and μ, the above equation becomes in terms of the functions ν and δ, as follows:

$$\nu(R^2-x)=\frac{\lambda}{\pi}\int_0^x\frac{\delta'(R^2-\xi)}{(x-\xi)^{1/2}}d\xi\,.$$

Here it should be noted that the prime denotes the differentiation with respect to ξ. Consequently this equation becomes by the transformation (3)

$$\nu(v)=-\frac{\lambda}{\pi}\int_0^{R^2}\frac{\delta'(u)}{(u-v)^{1/2}}du\,.$$

For convenience' sake we now introduce the non-dimensional quantities defined by

$$u^*=u/R^2,\qquad v^*=v/R^2.$$

Then

$$\nu(v^*)=-\frac{\lambda}{\pi R}\int_{v^*}^1\frac{\delta'(u^*)}{(u^*-v^*)^{1/2}}du^*.$$

Since, from the definition, $\nu=n-n_1$, the Gladstone-Dale equation gives

$$\nu=K(\rho-\rho_1).$$

Hence

$$\rho(v^*)-\rho_1=-\frac{\lambda}{\pi KR}\int_{v^*}^1\frac{\delta'(u^*)}{(u^*-v^*)^{1/2}}du^*. \tag{8}$$

This represents the relation between ρ and δ at a cross section vertical to the free-stream direction. Consider, for example, that the values of δ are known along the lines A—A′ in Fig. 5. Then the values of the density can be evaluated from this equation.

Before proceeding into the actual calculation for Eq. (8), we examine the behavior of the singularities occurring in the integrand. As seen immediately from the form of the integrand, the minus 1/2-order singularity develops at the point $u^*=v^*$, being integrable. One more singularity develops at the point $u^*=1$, corresponding to the shock wave. Applying Eq. (2) to the vicinity of the shock wave, we get

$$\delta^*(u)\simeq\frac{\nu(R^2)}{\lambda}\int_0^{R^2}\frac{dv}{(v-u)^{1/2}}$$
$$\simeq\frac{2\nu(R^2)}{\lambda}(R^2-u)^{1/2},$$

whence

$$\delta^{*\prime}(u)\simeq -\frac{\nu(R^2)}{\lambda(R^2-u)^{1/2}},$$

or

$$\delta^{*\prime}(u^*)\simeq -\frac{\nu(R^2)}{\lambda(1-u^*)^{1/2}}.$$

It follows from this form of $\delta^{*\prime}(u^*)$ that the integrand in Eq. (8) has the minu 1/2-order singularity at the point $u^*\simeq 1$ and is also integrable. To compute the density straightforwardly by use of Eq. (8), the numerical differentiation together with the numerical integration is required and then the error results mainly from this procedure. Therefore, the fringes must be produced as numerously as possible to reduce the error.

6. Measuring Results and Discussion

6.1 *The Patterns of Streamlines, Sonic Line and Equi-Local-Mach-Number Line*

The interferograms obtained for Models 1 and 2 at Mach number 4.3 were

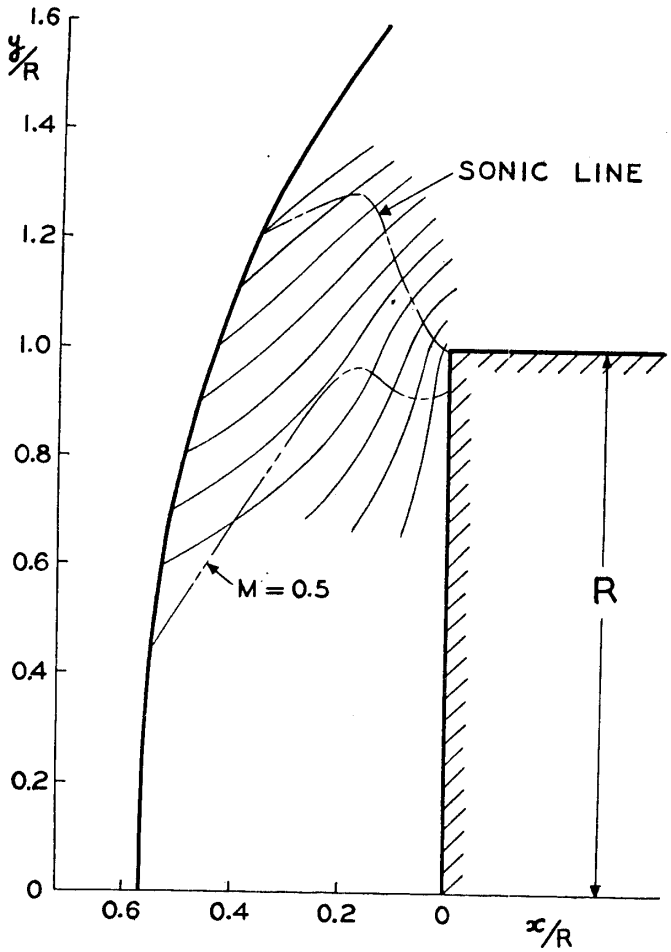

FIGURE 6. Shock wave, stream lines and equi-local-Mach-number lines for Model 1 at $M=4.3$.

analyzed by the method prescribed in the preceding section (Plates 4 and 5). On the basis of the isopicnics thus obtained, the stream lines were evaluated graphically in step-by-step procedure starting from the shock wave where flow directions can be determined from the observed shock pattern by the use of the shock theory. The sonic line and equi-local-Mach-number line ($M=0.5$) were obtained from the one dimensional stream tube considerations. These results are presented in Figs. 6 and 7. Since, at the vicinity of the axis and stagnation point, stream lines as well as isopicnics were obtained only with insufficient accuracy, the pattern of the stream lines was not sketched in Figs. 6 and 7.

Due to the results the regions with the Mach number lower than 0.5 occupies a considerably extensive part ahead of the nose in either case of Models 1 and 2. Recently Garabedian and Lieberstein [*10*] analyzed numerically the flow over a nearly spherical body at the Mach number 5.8, its contour being shown by broken line in Fig. 7. For the comparison with the present experimental results, the patterns of the shock wave and sonic line and the flow directions are also shown by broken lines and arrow marks, respectively, in Fig. 7. There exists a considerable difference in free-stream Mach number between these two cases. Nevertheless, the patterns of the shock wave and sonic line, and the flow direction are found

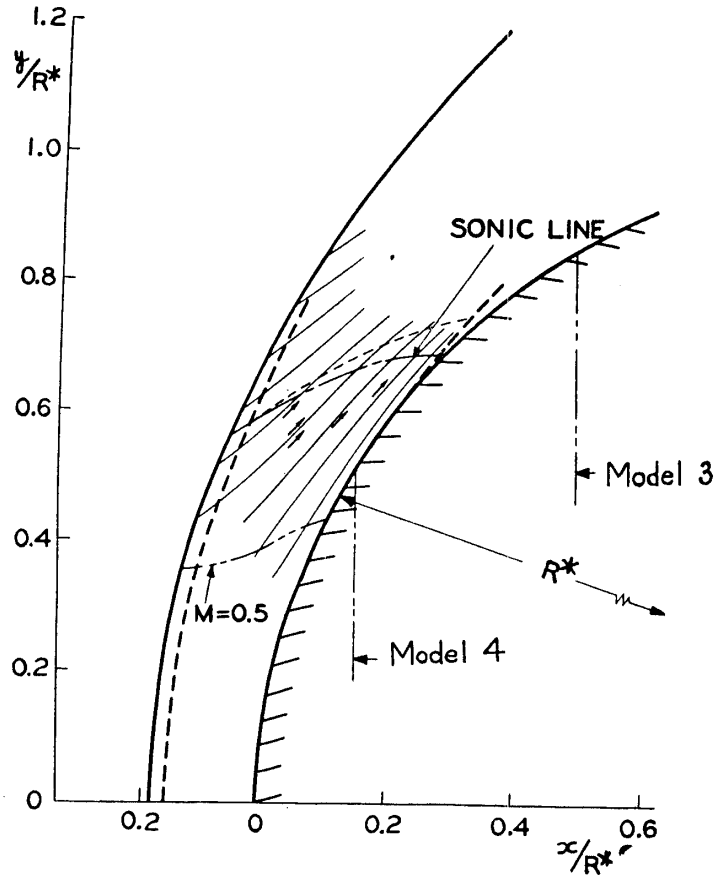

FIGURE 7. Shock wave, stream lines and equi-local-Mach-number lines for Model 2 at $M=4.3$. (Broken lines and arrow marks were reproduced from results of Ref. [*10*].)

to be very similar to each other. This implies that, for the case of an axially symmetric flow, the characteristic features of a hypersonic flow begin to appear at a lower Mach number than usually anticipated.

6.2 *Pressure Distribution on the Surface*

The pressures along the surface are presented in Figs. 8 and 9, respectively, for the cases of Models 1 and 2 when placed in the flow with the Mach number 4.3. The ordinate in Fig. 8 shows the distance measured along the surface from the nose, divided by the value at the sonic point. On the other hand, the ordinate in Fig. 9 shows the ratio θ of the arc length to the body radius. The abscissas in Figs. 8 and 9 show the ratio $p/p_{\max.}$ of the pressure of the stagnation one. For the comparison the present results are shown in Figs. 8 and 9, respectively, together with those obtained by Erassa and Wisenbaker [*6*] and by Oliver [*5*] at the Mach number 5.8. The theoretical values obtained in Reference [*10*] are also presented with full line in Fig. 9. As seen from these figures, the present results concerning $p/p_{\max.}$ are found to be in good agreement with those obtained either theoretically or experimentally for the case of the Mach number 5.8. This will provide further justification for the previous argument that for the case of axially symmetric flow characteristic features of a hypersonic flow begin to appear at a lower Mach number than usually anticipated.

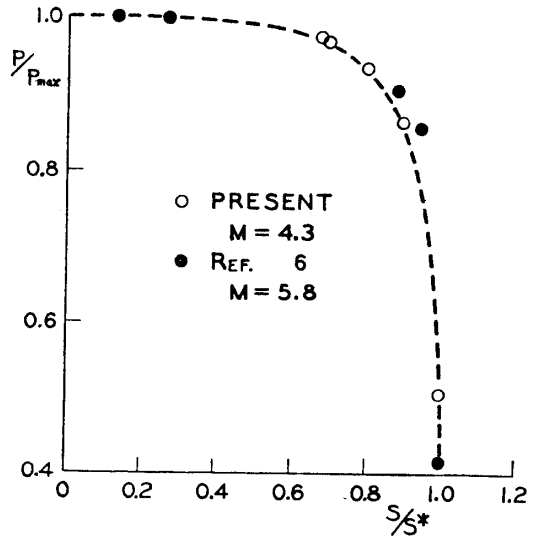

FIGURE 8. Surface pressure distribution for Model 1.

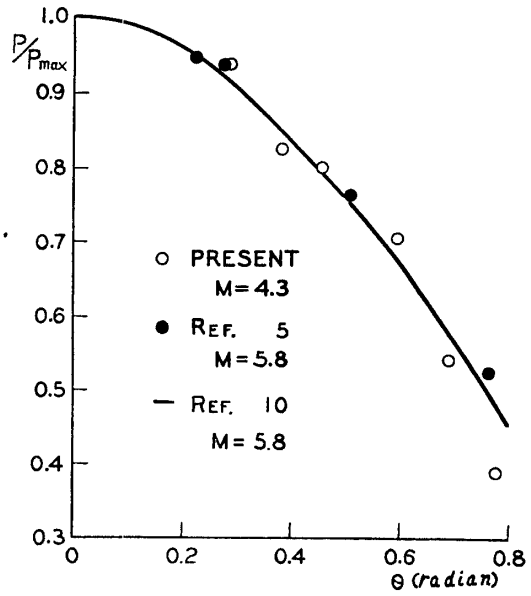

FIGURE 9. Surface pressure distribution for Model 2.

6.3 *Relation Between the Radius of Curvature and the Shock-Wave Detachment Distance*

The shock-wave patterns were obtained for all models by either interferometer or schlieren metheod over the Mach number range from 3.76 to 4.78. Several examples of the photographs taken by the schlieren method are presented in Plates 7–10. The shock-wave detachment distance at the nose, δ/R, divided by the reference length R is plotted in Fig. 10 against the free-stream Mach number M.

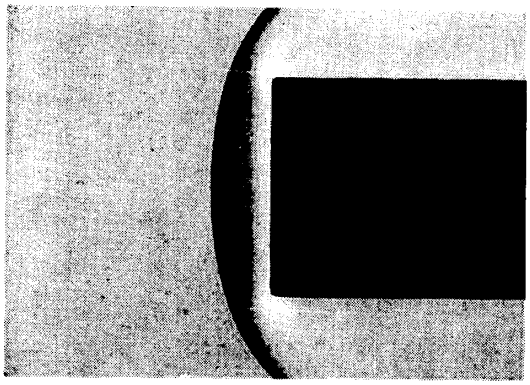

PLATE 7. $M=4.30$

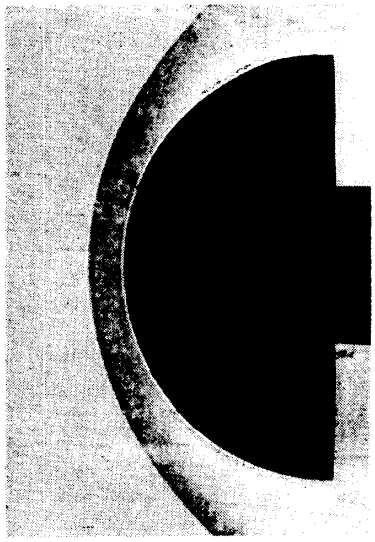

PLATE 8. $M=4.26$

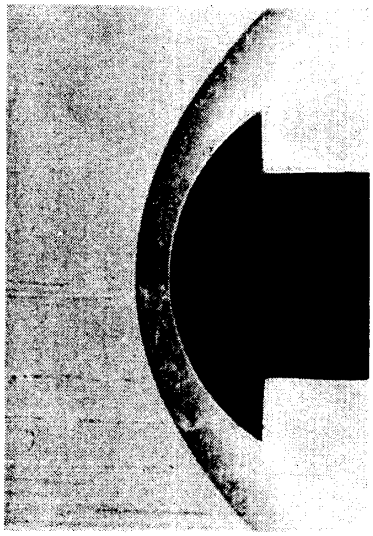

PLATE 9. $M=4.31$

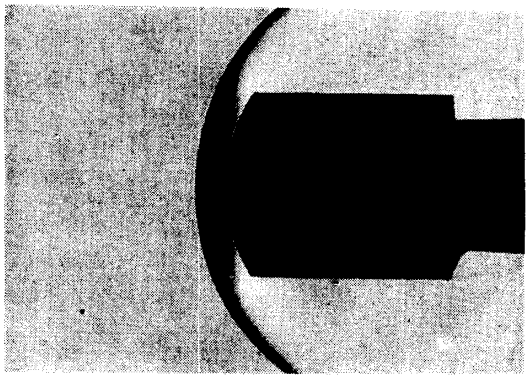

PLATE 10. $M=4.27$

Here the reference length is selected as a radius of maximum cross section vertical to the axis of body (Fig. 1). As seen from Fig. 10, the values of δ/R depend remarkably on the figure of bodies.

When the radius of curvature, R_S, of the shock wave at the nose is assumed as a reference length, however, the relations of δ/R_S versus M are found to be nearly independent of the figure of bodies (Fig. 11). Here the width of plots represents the uncertainty of those values mainly due to the error involved in the value of R_S. It should be worth noting that the value of δ/R_S is nearly independent of whether the nose is flat or spherical. Due to the fact, the radius of curvature of the shock wave may be concluded to be an important reference length pertinent to the flow field.

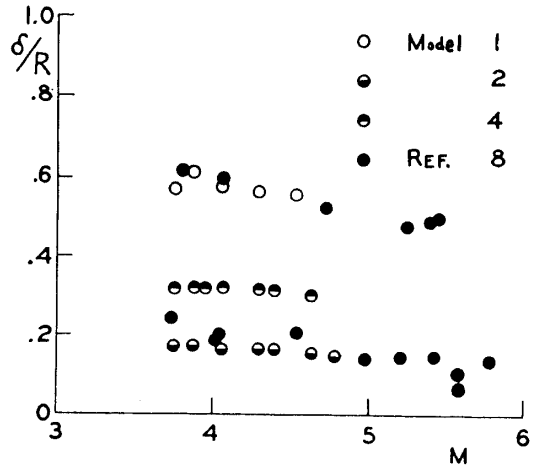

FIGURE 10. Shock-wave detachment distance referred to maximum frontal radius, R, versus free-stream Mach number M.

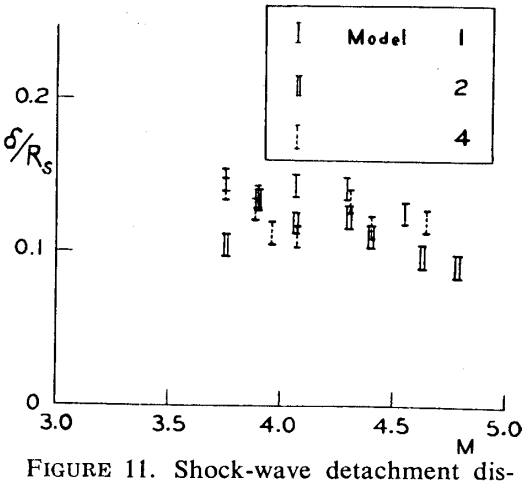

FIGURE 11. Shock-wave detachment distance referred to radius, R_s, of curvature of shock wave versus free-stream Mach number M.

6.4 *Sonic Point on the Surface*

The shock-wave pattern for Model 3 was observed but the results were not presented in the preceding section, because they were found very close to the results for the case of Model 2. Models 3 and 4 have the same radius as Model 2 (Fig. 1). There exists a distinct difference between the figures of Models 3 and 4. As seen from Fig. 7, the former is cut off downstream of the sonic point on the surface of Model 2 when $M=4.3$, while the latter upstream of this point. For these models the ratio, δ/R^*, of the shock-wave detachment distance to the body radius R^* is plotted in Fig. 12 against the free-stream Mach number M. Since the values of R^* were the same as for these models, we can see from Fig. 12 that the detachment distance δ is nearly independent of the position of the shoulder, at least,

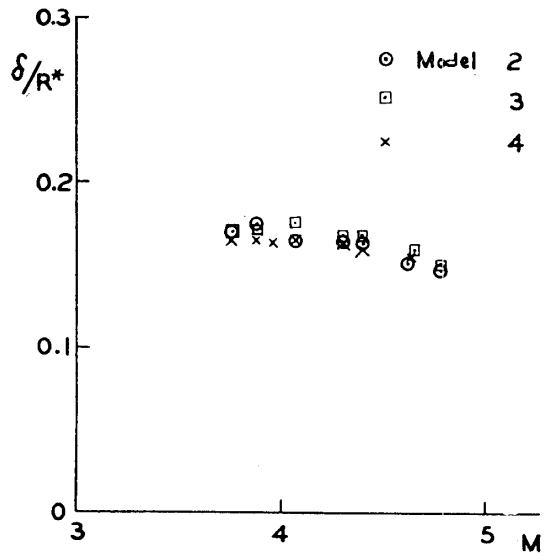

FIGURE 12. Shock-wave detachment distance referred to body radius versus free-stream Mach number M.

over the range of Mach numbers under investigation. This result leads to the conjecture that the shock-wave detachment distance may be to zero order determined only from the flow behavior near the nose, independently of that near the sonic point.

Concluding Remarks

In the present experiment the flows over several bodies of revolution were observed over Mach number range from 3.76 to 4.78 by the interferometer and schlieren method. The main results may be summarized as follows:

(1) The characteristic features of a hypersonic flow begin to appear in the flow over the blunt-nosed body of revolution at the lower Mach number rather than usually anticipated. Indeed, the non-dimensional surface pressure, shock-wave pattern, sonic line pattern and flow directions were found to show strongly such a trend.

(2) The region with local Mach number lower than 0.5 was confirmed to spread extensively over a disturbed flow ahead of the nose.

(3) The shock-wave detachment distance is nearly independent of the nose shape when referred to the radius of curvature of the shock wave. Therefore, the radius of curvature of the shock wave seems to be most important one as a reference length of the flow fields.

(4) For the bodies with the same nose radius, the shock-wave detachment distances are nearly independent of the position of their shoulders.

Acknowledgement

The author wishes to express his sincere thanks to Profs. Sandi Kawada and Ryuma Kawamura for their helpful advices and encouragement throughout this investigation. The author also wishes to express his hearty gratitude to Messrs. Yujiro Naito and Katsuyuki Hunabiki for their eager assistence.

Department of Aerodynamics
Aeronatical Research Institute
University of Tokyo, Tokyo,
October 22, 1958

References

[1] Oguchi, H.: Hypersonic Flow Near the Forward Stagnation Point of a Blunt-Nosed Body of Revolution, Aero. Res. Inst., Univ. of Tokyo, Report No. 337 (Vol. 24, No. 8) 1958.

[2] Li, T. Y. and Geiger, R. E.: Stagnation Point of a Blunt Body in Hypersonic Flow, Jour. Aero. Sci., Vol. 24, No. 1, 1957, p 25.

[3] Lighthill, M. J.: Dynamics of a Dissociating Gas. Part I., Equilibrium Flow, Jour. Fluid Mech., Vol. 1, Part 1, 1957, p 1.

[4] Hida, K.: An Approximate Study on the Detached Shock Wave in Front of a Circular Cylinder and a Sphere, Jour. Phys. Soc. of Japan, Vol. 8, No. 6, 1955, p 79.
[5] Oliver, R. E.: An Experimental Investigation of Flow About Simple Blunt Bodies at a Nominal Mach Number of 5.8, Jour. Aero. Sci., Readers' Forum, Vol. 23, No. 2, 1956, p 177.
[6] Lees, L.: Recent Developments in Hypersonic Flow, Jet Propulsion, Vol. 27, 1957, p 1162.
[7] Vas, I. E., Bogdonoff, S. M. and Hammitt, A. G.: An Experimental Investigation of the Flow Over Simple Two-Dimensional and Axial Symmetric Bodies at Hypersonic Speeds, Jet Propulsion, Vol. 28, 1958, p 97.
[8] Serbin, H.: Supersonic Flow Around Blunt Bodies, Jour. Aero. Sci., Readers' Forum, Vol. 25, No. 1, 1958, p 58.
[9] Oswatitsch, K.: Ähnlichkeitsgesetze für Hyperschallströmung, Z. A. M. P., Vol. 2, 1951, p 249.
[10] Garabedian, P. E. and Lieberstein, H. M.: On the Numerical Calculation of Detached Bow Waves in Hypersonic Flow, Jour. Aero. Sci., Vol. 25, No. 2, 1958, p 109.
[11] Oguchi, H. and Naito, Y.: The Experiments on the Characteristics of a Variable Geometry Diffuser and the Improvement of the Starting Condition by its Application with a Movable Nozzle, Proc. 7th Japan National Cong. for Appl. Mech., 1957, p 189.
[12] Ladenburg, R. E. and Others: Physical Measurements in Gas Dynamics and Combustion, High Speed Aerodynamics and Jet Propulsion, Vol. IX, Princeton Univ. Press, 1954.
[13] Howarth, L.: Modern Developments in Fluid Dynamics, High Speed Flow, Vol. II, Oxford, 1953.
[14] Ames Research Staff: Equations, Tables, and Charts for Compressible Flow, NACA TR 1135, 1953.
[15] Ladenburg, R., Winckler, J. and Van Voorhis, C. C.: Interferometric Studies of Faster Than Sound Objects in a Free, Homogeneous, Supersonic Air Stream, Phys. Review, Vol. 74, No. 11, 1948, p 1359.